High spatial resolution quantitative micromagnetics (invited)

M. R. Scheinfein, J. Unguris, D. T. Pierce, and R. J. Celotta
National Institute of Standards and Technology, Gaithersburg, Maryland 20899

Magnetization profiles at surfaces are observed with scanning electron microscopy with polarization analysis (SEMPA). This technique allows for quantitative analysis of the vector magnetization profile with 70 nm spatial resolution. Magnetization profiles in surface Néel walls which terminate bulk 180° Bloch walls at surfaces have been calculated by solving the micromagnetic equations using energy minimization. The micromagnetic calculations show that the surface Néel wall penetrates a distance from the surface comparable to a Bloch wall width and that the surface Néel wall width is at least twice the bulk Bloch wall width. The dependence of the domain wall magnetization on sample thickness is calculated for Fe, and model predictions of the wall widths that would be determined by transmission Lorentz microscopy are compared with the experimental results. The magnetic field outside of the sample, which gives rise to contrast with the Bitter technique and magnetic force microscopy (MFM), is a complicated superposition of contributions from both bulk and surface walls. Moreover, a strong mutual interaction between the sample and the MFM tip may alter the sample magnetization.

INTRODUCTION

High spatial resolution imaging of magnetic microstructure has important ramifications for both fundamental studies of magnetism and for the technology surrounding the magnetic recording industry. Ferromagnetic length scales vary widely due to the variation in the physical parameters which characterize ferromagnetic systems. Most methods used for the observation of magnetic microstructure rely on the magnetic fields present in ferromagnetic systems. In the Bitter method[1] fine magnetic particles in solution are placed on the surface where they agglomerate in the fringe fields produced at domain walls. The agglomerated particles are usually imaged with optical techniques, and the spatial resolution is about 1 μm. In Lorentz electron microscopy, an incident beam of electrons is deflected by the net magnetic field in or near the specimen. In reflection Lorentz electron microscopy[2,3] bulk magnetic samples can be observed with 1 μm spatial resolution. In transmission Lorentz electron microscopy,[3-5] where thin samples are required ($t < 0.3\ \mu$m), extremely high spatial resolution (0.01 μm) observation of magnetic microstructure is possible. Techniques employing transmission electron microscopes (TEMs) yield magnetic microstructural information averaged over the entire electron trajectory as it traverses the sample. A new technique, magnetic force microscopy (MFM), achieves contrast through the magnetostatic interaction between the sample fringe fields and a magnetized ferromagnetic tip. MFM can be used to locate domain walls and analyze them with high spatial resolution (100 nm).[6] Interactions between the tip and the sample may place an upper limit on the ultimate spatial resolution achievable with this technique. All of these methods derive image contrast from the probe coupling to the magnetic fields of the ferromagnetic sample and hence only offer an indirect measure of the sample magnetization. In contrast, the magneto-optic Kerr effect[7] directly measures the sample magnetization by determining the rotation of the plane of the polarization of light upon reflection. As an optical method, its spatial resolution ($> 0.25\ \mu$m) is limited by diffraction to optical wavelengths.

Scanning electron microscopy with polarization analysis (SEMPA) is a relatively new technique which directly measures the magnetization for ferromagnetic transition metals.[8-10] The principle of the technique is illustrated in Fig. 1(a). A beam of focused electrons from an electron microscope incident upon a ferromagnetic sample excites secondary electrons near the surface. The secondary electrons retain their spin orientation as they leave the sample surface, and are efficiently collected and transported to an electron-spin polarization analyzer.[11,12] SEMPA can therefore measure the magnetization directly, as the electron-spin polarization of the emitted secondaries is characteristic of the net spin density of the valence band in the solid, and the net spin density is related to the sample magnetization for most ferromagnetic materials. A map of the surface vector magnetization is made by rastering the incident high energy focused electron beam across the sample surface, and spin analyzing the emitted polarized secondary electrons. We si-

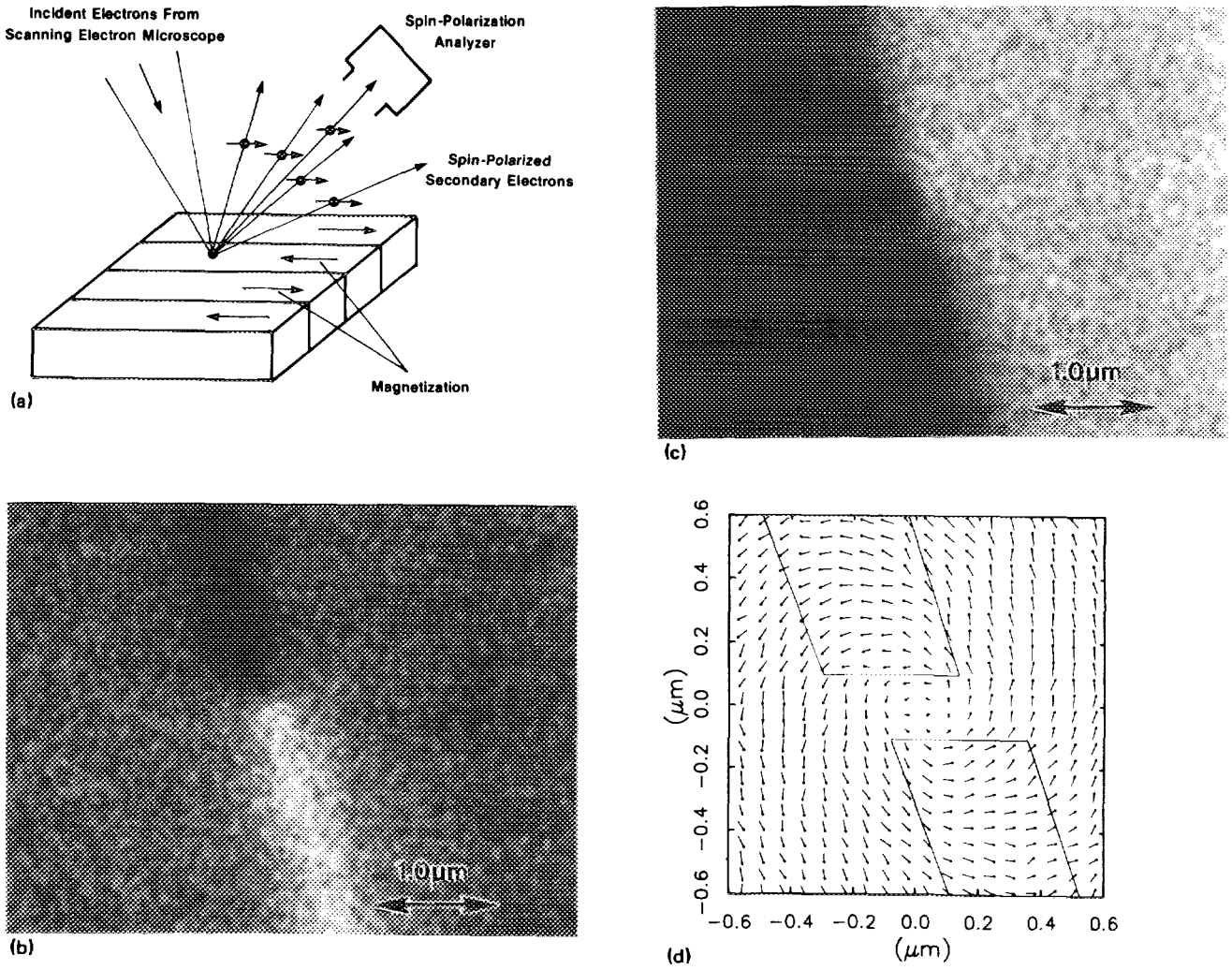

FIG. 1. (a) Schematic representation of scanning electron microscopy with polarization analysis (SEMPA). (b) SEMPA image of the horizontal and (c) vertical component of the magnetization in a Co based ferromagnetic glass. White (black) is magnetization in the positive (negative) directions. (d) An enlarged view of the surface magnetization vector field near the magnetic singularity seen in (b). The boxes are meant only to schematically indicate the surface wall locations.

multaneously acquire two components of the magnetization signal, along with the conventional secondary electron intensity signal. In our apparatus,[10] two orthogonal spin detectors are present. The two spin detectors allow for all three components of the vector magnetization to be analyzed without reorienting the sample. We typically achieve a spatial resolution of 70 nm in SEMPA.

OBSERVATION OF MAGNETIC MICROSTRUCTURE USING SEMPA

SEMPA is useful for imaging magnetic domains in a wide class of materials.[10,13] Here, we emphasize both the high spatial resolution and the quantitative aspects of SEMPA. The horizontal component of the magnetization of a surface Néel wall which terminates a bulk 180° Bloch wall in a Co-based ferromagnetic glass (Allied 2705M, $Co_{69}Fe_4Ni_1Mo_2B_{12}Si_{12}$) is shown in Fig. 1(b). The vertical component of the magnetization is shown in Fig. 1(c). Both the horizontal and vertical components of the magnetization are in the plane of the figure. These images were acquired simultaneously, and are 6.4 μm across. In both images, white (black) corresponds to magnetization pointing in the positive (negative) axis direction, to the right in Fig. 1(b) and up in Fig. 1(c). There was no magnetization pointing out of the plane in this region. In Fig. 1(d), an enlarged view of the vector magnetization at the center of the Néel wall, where the surface wall magnetization orientation changes, is shown. The length of the arrows is proportional to the magnitude of the in-plane component of the magnetization vector, while the direction of the arrows indicates the direction of the vector field. The features of particular interest are (1) the presence of the surface Néel walls and the offset of the walls, and (2) the presence of the magnetic singularity at the intersection of the surface Néel walls at the center of the figure.[14-16]

We compared the measurements with simulations based upon the solution to the micromagnetic equations.[17-19] In our simulations, the continuous magnetization is approxi-

mated by dividing the ferromagnet into a finite number of cells, each with a discrete magnetization. The magnetization within each cell is affected by that of the nearest-neighbor cells through the exchange interaction (i.e., exchange in the mean field sense), and by all other cells through the long range magnetostatic interaction. Either cubic or uniaxial magnetocrystalline anisotropy fields are included.

In each cell we vary the direction of the magnetization iteratively to minimize the energy. We do not use the alternative method of directly integrating the Landau–Lifshitz–Gilbert (LLG) equations in time. For soft magnetic materials, the final energy of the relaxed system is independent of the damping parameter used in the LLG equation, and our method yields similar results to the integration of the LLG equation.[15,20] Our calculation has as input the material parameters, e.g., the mean field exchange constant A, the magnetocrystalline anisotropy constant K (of either cubic or uniaxial structure), the saturation magnetization M_s, and such geometrical parameters as the film thickness and the associated boundary conditions. The output of the calculation is the orientation of the magnetization at each location in the mesh and the energy of the final configuration.

Typical results from a simulation are illustrated for a 500-nm-thick Fe crystal in Fig. 2. The cross section of the film lies in the x-y plane, and the 180° domain wall being modeled has the magnetization to the left of the wall going into the figure ($-z$), and the magnetization on the right of the wall coming out of the figure ($+z$). Figure 2(a) is a cross section through the 180° domain wall in the Fe film. The parameters used in the simulation are $A = 2.0\times10^{-6}$ erg/cm, $K = 4.7\times10^{5}$ erg/cm^3, and $M_s = 1714$ emu/cm^3. The bulk Bloch wall running vertically through the center of Fig. 2(a) is clearly visible. On the surface of the film ($y = 0$), the Bloch wall terminates in a surface Néel wall in order to minimize the magnetic stray field energy. In Fig. 2(b) the calculated magnetization components at the surface are shown for this wall configuration. This is the magnetization profile that will be measured in a SEMPA experiment where the sampling depth is on the order of nanometers.[21] In Fig. 2(c), we show the calculated bulk magnetization ($y = 250\,nm$) components. Immediately evident from Figs. 2(b) and 2(c) is that the surface Néel wall (M_x) is asymmetric and about a factor of 2 wider than the bulk Bloch (symmetric) wall (M_y). Also evident is a distinct offset, by a distance Δ, between the peak in the magnetization profile of the surface Néel wall (M_x) and the bulk Bloch wall (M_y). This offset can be measured from SEMPA images, such as Fig. 1(b), which shows a surface wall changing its sense of rotation. For a continuous bulk Bloch wall, the Néel wall at the surface either falls to the left or the right of the bulk Bloch wall, giving an offset of 2Δ between the two surface Néel walls.[15]

It is of interest to compare bulk wall widths determined from the micromagnetic calculations with those determined by the classical variational method[25] for uniaxial crystals. Once the angular dependence of the magnetization profile has been determined, the maximum slope at the center of the wall $d\Theta/dx = (K/A)^{1/2}$ is used to define a wall width of $\pi(A/K)^{1/2}$. We found our results to differ from the classical

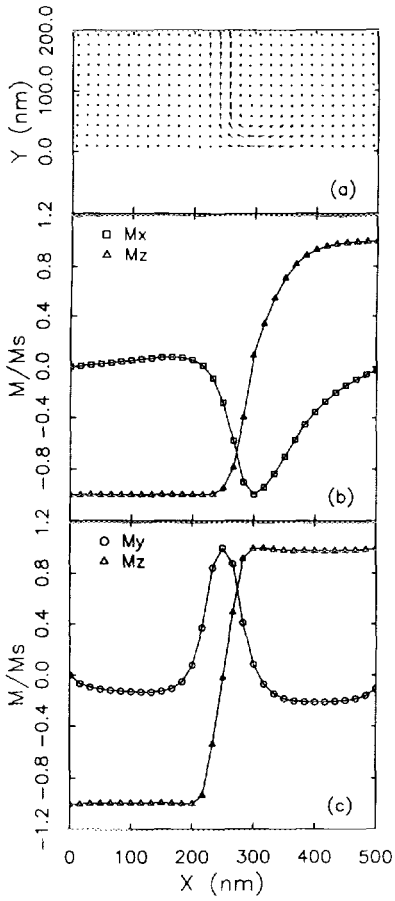

FIG. 2. (a) Cross section of an Fe crystal 180° Bloch wall as simulated by solving the micromagnetic equations. The magnetization is into the page on the left of the wall and out of the page to the right of the wall. The bulk Bloch wall, indicated by vertical arrows in the interior, is terminated at the surface by a surface Néel wall. (b) Surface magnetization profile as would be measured in SEMPA. (c) Bulk magnetization profile.

model by less than 5%. However, the wall width definition which leads to the $\pi(A/K)^{1/2}$ result is only meaningful for ferromagnets possessing uniaxial magnetocrystalline anisotropy and highly symmetric wall profiles. We use as our definition of the wall width the distance in which the wall magnetization, M_x in Fig. 2(b) and M_y in Fig. 2(c) passes from 10% to 10% of its maximum value. This measure of the wall width guarantees that walls with very different magnetization profiles will have the magnetization rotate through identical angles through the wall.

Returning to Fig. 2(a), we see that the depth of the magnetic disturbance propagated into the bulk at the surface is on the order of a bulk Bloch wall width. This means that, for all but the hardest materials, the magnetic contrast measured from the surface in SEMPA, and that measured by the magneto-optic Kerr effect, with a probing depth of about 10–15 nm, should be nearly identical. This has been qualitatively confirmed,[22] and a detailed comparison of the two techniques will be published.[23] Furthermore, we find that

the widths of the surface Néel walls, as defined above, are at least two times as large as the bulk Bloch wall widths for ferromagnets which are thick enough to support bulk Bloch walls. For thin films which support vortexlike structures characteristic of asymmetric Bloch walls,[18,24] the width of the surface Néel wall is limited by the film thickness.[18,23,24]

TRANSMISSION LORENTZ ELECTRON MICROSCOPY

We have simulated the effect of thickness on the domain walls found in crystalline Fe and uniaxial Permalloy.[23] In Figs. 3(a)–3(b), cross sections through 180° domain walls in Fe are shown for films of varying thickness. The thicknesses of the Fe films in Figs. 3(a) and 3(b) are 50 and 300 nm, respectively. The magnetocrystalline anisotropy has cubic symmetry. The asymmetric Bloch walls[18,24,26] with the well-defined vortex structure at the center of the film is clearly observed. The domain wall magnetization configuration is a strong function of the thickness of the sample for thicknesses small enough that the long range magnetostatic interactions couple the two sides of the film. As the film thickness is increased, the wall expands until the vortex structure at the center is effectively broken. On further increasing the film thickness, the bulk Bloch wall in the film center only lengthens. Until the film reaches a thickness where the asymmetric Bloch wall separates into a well-formed bulk Bloch wall, the surface Néel wall width will be a function of the film thickness.

The wall widths as measured in TEM Lorentz can be correlated with the magnetization perpendicular to the beam averaged over the film thickness. We have calculated the apparent wall widths expected from transmission Lorentz microscopy for Fe as a function of sample thickness. These are shown by the solid points in Fig. 3(c), where the solid line is a fit to guide the eye. The results from the TEM Lorentz experiments[27] are also shown for thicknesses up to 300 nm. The wall width increases as a function of thickness until the asymmetric wall profile breaks apart, and more of the Lorentz deflection contrast originates with the narrower bulklike Bloch wall in the interior, causing the width expected from the measurement to decrease. The transmitted electrons from thicker films have greatly degraded spatial resolution due to multiple scattering and beam attenuation. Therefore, measurements of Fe domain walls cannot enter the range of film thicknesses where the bulk Bloch wall is fully developed.

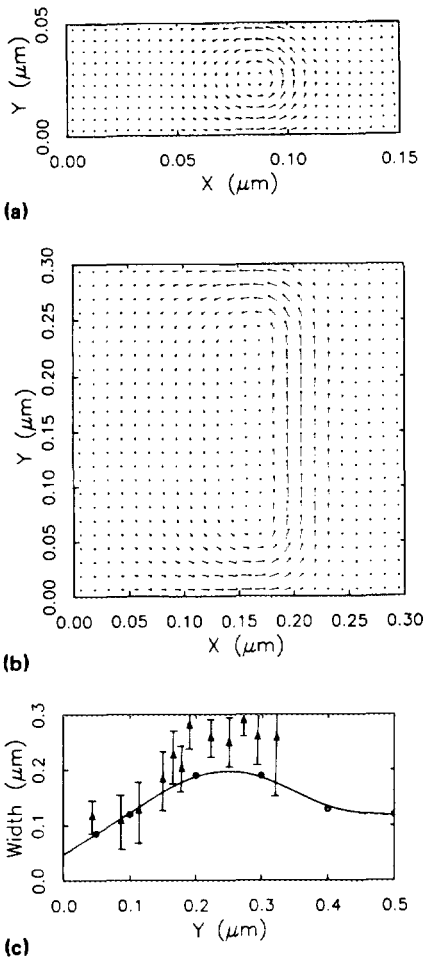

FIG. 3. Domain walls shown in cross section for an Fe single crystal calculated for different thickness films, (a) 50 nm and (b) 300 nm. The calculated (solid circles) and measured (Ref. 27) (with error bars) wall widths as determined by TEM Lorentz microscopy as a function film thickness for Fe (c).

BITTER METHODS

The Bitter technique, in which the ferromagnetic particles agglomerate in the stray fields near domain walls, is useful for decoration of domain walls and determining the domain configuration. Attempts have been made to measure the structure of the walls, and simple models of Bloch wall widths as determined by ferromagnetic fluids have been given.[28] However, real field profiles have contributions from both the interior bulk Bloch wall and the surface Néel wall. In Fig. 4, the vertical component of the magnetic field is shown at two heights, 16 and 800 nm, above the Fe sample surface. It is evident that the peak in the field profile is not solely associated with the bulk Bloch wall or the surface Néel

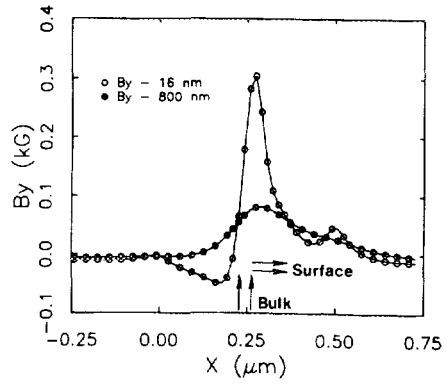

FIG. 4. The vertical component of the magnetic field B_y at two heights above the Fe surface near a domain wall. The arrows indicate the actual position of the domain walls in the bulk and on the surface.

wall. The shape of the field is also a complicated function of the superposition of the fields generated by the divergence in the magnetization.

One way of visualizing the fields generated near where a surface intersects a domain wall is to assume that the bulk Bloch wall acts like a magnetic dipole with the top pole located a Bloch wall width beneath the surface. The surface Néel wall could be viewed as a magnetic dipole in the plane of the surface oriented at right angles to the dipole in the bulk. By superimposing the effects of both dipoles, the qualitative behavior of the resulting field profile can be gleaned. The slight positive bump near $x = 0.50\ \mu$m results from the magnetic charge near the end of the surface dipole, as does the slight negative bump near $x = 0.15\ \mu$m. The largest peak is shifted to the right of the bulk Bloch wall by the negative component contributed by the surface wall. The separation of the bulk and surface components from a Bitter measurement is extremely difficult, and for ferromagnetic materials like Fe the walls are smaller than the optical probes used to observe the agglomerated particles.

MAGNETIC FORCE MICROSCOPY

The magnetic force microscope couples a ferromagnetic tip to the fringe fields emanating from a ferromagnetic specimen. The observed magnetic contrast is a complicated function of the magnetic tip shape, material, and distance from the sample.[6]

Figure 5 shows a simulation, based on our micromagnetics models, of an Fe tunneling tip scanning across an asymmetric Bloch wall in a 200-nm-thick zero-magnetostriction Permalloy film. The tip magnetization is that of bulk Fe, $M_s = 1714$ emu/cm^3. In this simulation, the tip moments were not allowed to reconfigure during the energy minimization scheme. The parameters of this Permalloy film are $A = 1 \times 10^{-6}$ erg/cm, $M_s = 800$ emu/cm^3, and $K = 1000$ erg/cm^3. In this two-dimensional model the tip is assumed infinite in the z direction so as not to break the two-dimensional wall symmetry. As the ferromagnetic tip (knife) located 20 nm above the surface is scanned from right to left in Figs. 5(a)–5(c), the wall magnetization couples directly with the tip, closing the flux through the tip itself. The wall is effectively dragged along by the tip as it is scanned across the wall, as has been experimentally observed[29] for a Ni tip scanning a Permalloy film. The unperturbed wall profile is shown in Fig. 5(d). Notice also that the center of the asymmetric Bloch wall vortex changes its vertical position as the tip is scanned across the wall.

Although this simulation is a two-dimensional approximation and is not expected to yield quantitative information about the specific contrast mechanism seen in a particular MFM measurement, qualitatively it is easily seen that a full micromagnetic simulation will be essential in order to deconvolve the effect of the probe from observations of domain walls in soft materials. Furthermore, in order to decrease the effect of the tip on the magnetization within the wall, the tip must be moved away from the surface, thereby decreasing spatial resolution, and/or the tip magnetization must be decreased, thereby decreasing image contrast.

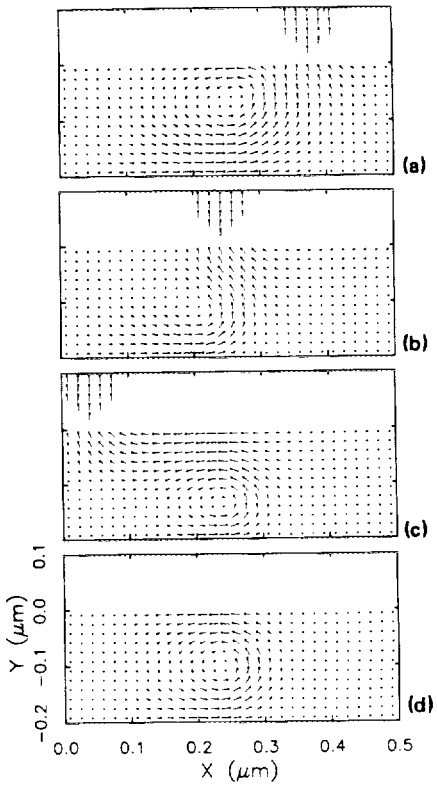

FIG. 5. An Fe tip is scanned across the surface of a thin Permalloy film (a)–(c) in this two-dimensional simulation of a magnetic force microscope. The tip is located 20 nm above the surface. The unperturbed wall configuration is shown in (d).

CONCLUSION

We have demonstrated that scanning electron microscopy with polarization analysis is an effective tool for investigating surface domain wall microstructure on the 70 nm length scale. SEMPA provides quantitative, high spatial resolution measurements of surface domain wall structures. The solution of the micromagnetic equations can give further insight in the behavior of domain walls interior to the sample. The micromagnetic models were used to investigate domain wall contrast mechanisms in TEM Lorentz, Bitter, and magnetic force microscopy and the limits of these techniques were discussed.

ACKNOWLEDGMENTS

This work was supported in part by the Office of Naval Research. Thanks to all of the members of the Electron Physics Group for support. Thanks to Professor H. C. Siegmann and Dr. R. Victora for useful conversations.

[1] F. Bitter, Phys. Rev. **38**, 1903 (1931).
[2] D. E. Newbury, D. E. Joy, P. Echlin, C. E. Fiori, and J. I. Goldstein, *Advanced Scanning Electron Microscopy and X-ray Microanalysis* (Plenum, New York, 1986).
[3] K. Tsuno, Rev. Solid State Sci. **2**, 623 (1988).
[4] J. P. Jacubovics, *Electron Microscopy in Materials Science Part IV*, edited by E. Ruedl and U. Valdre (Commission of European Communities, Brussels, 1973), p. 1305.
[5] J. N. Chapman, J. Phys. D **17**, 623 (1984).
[6] A. Wadas and P. Grutter, Phys. Rev. B **39**, 12013 (1989).

[7] J. Kranz and A. Z. Hubert, A. Angew. Phys. **15**, 220 (1963).
[8] K. Koike, H. Matsuyama, H. Todokoro, and K. Hayakawa, Scanning Microsc. Suppl. **1**, 241 (1987).
[9] G. G. Hembree, J. Unguris, R. J. Celotta, and D. T. Pierce, Scanning Microsc. Suppl. **1**, 229 (1987).
[10] M. R. Scheinfein, J. Unguris, M. H. Kelley, D. T. Pierce, and R. J. Celotta (to be published.)
[11] D. T. Pierce, R. J. Celotta, M. H. Kelley, and J. Unguris, Nucl. Instrum. Methods A **266**, 550 (1988).
[12] M. R. Scheinfein, D. T. Pierce, J. Unguris, J. J. McClelland, and R. J. Celotta, Rev. Sci. Instrum. **60**, 1 (1989).
[13] J. Unguris, M. R. Scheinfein, D. T. Pierce, and R. J. Celotta, in *Chemistry and Physics of Solid Surfaces VII*, edited by R. Vanselow and R. Howe (Springer, Berlin, 1990) (in press).
[14] A. Hubert, J. Phys. (Paris) Colloq. **49**, C8-1865 (1988).
[15] M. R. Scheinfein, J. Unguris, R. J. Celotta, and D. T. Pierce, Phys. Rev. Lett. **63**, 668 (1989).
[16] M. R. Scheinfein, J. Unguris, D. T. Pierce, and R. J. Celotta, in *Magnetic Properties of Low Dimensional Systems*, edited by L. Falicov (Springer, Berlin, 1990) (in press).
[17] W. F. Brown, *Micromagnetics* (Kreiger, Huntington, NY, 1978).
[18] A. E. LaBonte, J. Appl. Phys. **40**, 2450 (1969).
[19] M. E. Schabes and H. N. Betram, J. Appl. Phys. **64**, 1347 (1988).
[20] C. C. Shir, J. Appl. Phys. **49**, 3413 (1978).
[21] D. Penn, S. P. Apell, and S. M. Girvin, Phys. Rev. Lett. **55**, 518 (1985).
[22] A. Hubert (private communication).
[23] M. R. Scheinfein, P. Ryan, and J. Unguris (to be published).
[24] A. Hubert, Phys. Status Solidi B **32**, 519 (1969).
[25] S. Chickazumi, *Physics of Magnetism* (Wiley, New York, 1959).
[26] A. Aharoni, J. Appl. Phys. **46**, 914 (1975).
[27] T. Suzuki and K. Suzuki, IEEE Trans. Magn. **MAG-13**, 1505 (1977).
[28] U. Hartmann, J. Magn. Magn. Mater. **68**, 298 (1987).
[29] H. J. Mamin (private communication).